

Electron conduction in magnetized neutron star envelopes

A. Y. Potekhin

Ioffe Physical-Technical Institute, Politekhnikeskaya 26, 194021 St. Petersburg, Russia (palex@astro.ioffe.rssi.ru)

Received 11 May 1999 / Accepted 25 August 1999

Abstract. Practical expressions are derived for evaluation of electrical and thermal conductivities and thermopower of degenerate electrons in the outer envelopes of neutron stars with magnetic fields. All tensor components of the kinetic coefficients are calculated (those related to conduction along and across magnetic field and to the Hall currents). The kinetic coefficients are presented as energy averages of expressions containing energy dependent effective relaxation times of two types, associated either with longitudinal or with transverse currents. The calculation is based on the effective scattering potential proposed in the previous paper, which describes the electron-ion and electron-phonon scattering, taking into account correlation effects in strongly coupled Coulomb liquid and multi-phonon scattering in Coulomb crystal, respectively. Analytic fitting formulae are devised for the effective relaxation times at arbitrary field strength. Basing on these results, we calculate the transport coefficients at various temperatures, densities, and magnetic fields pertinent to the neutron star envelopes.

Key words: stars: neutron – dense matter – conduction – magnetic fields

1. Introduction

Transport properties of neutron star envelopes determine many aspects of neutron-star evolution. For instance, the thermal conductivity in the outer envelope affects cooling of a neutron star and its radiation spectra (e.g., Gudmundsson et al. 1983; Page 1997; Potekhin et al. 1997). The electrical conductivity is the basic quantity for the studies of magnetic-field evolution (e.g., Muslimov & Page 1996; Urpin & Kononov 1997; Konar & Bhattacharya 1997), which in turn affects thermal evolution (Miralles et al. 1998). The thermopower determines a variety of thermomagnetic phenomena (Urpin & Yakovlev 1980b; Urpin et al. 1986; Shibazaki et al. 1989; Yabe et al. 1991).

In the outer envelopes of neutron stars, the transport coefficients are mainly determined by the processes of electron scattering off strongly correlated ions. General formalism for calculating kinetic properties of strongly coupled Coulomb plasmas was developed by Hubbard & Lampe (1969) and Flowers & Itoh (1976) (see references to earlier results therein). Yakovlev & Urpin (1980) derived approximate analytic expressions, which

were confirmed later in more elaborate calculations by Raikh & Yakovlev (1982), Itoh et al. (1983), and Nandkumar & Pethick (1984). Itoh et al. (1984, 1993) improved the results of Yakovlev & Urpin (1980) and Raikh & Yakovlev (1982) in the solid crust by taking into account finite sizes of atomic nuclei (which may be important in the inner crust) and the Debye–Waller factor (which describes reduction of electron-phonon scattering rate due to background lattice vibrations). The Debye–Waller factor proved to be important at temperature T close to the melting temperature of a Coulomb crystal, T_m , or at sufficiently high densities where zero-point lattice vibrations are strong. Detailed numerical and analytic calculations by Baiko & Yakovlev (1995, 1996) were in reasonable agreement with Itoh et al. (1984, 1993).

Magnetic fields in the neutron-star envelopes complicate electron transport making it, particularly, anisotropic. The field strengths of radio pulsars range from $B \sim 10^8$ G to $B > 10^{13}$ G, with typical value $B \sim 10^{12}$ G (Taylor et al. 1993). Some X-ray pulsars and soft gamma repeaters are probably magnetars – neutron stars with $B \sim 10^{14} - 10^{15}$ G, as suggested by Thompson & Duncan (1995) and supported by recent observations (Vasishth & Gotthelf 1997; Gotthelf et al. 1999; Kouveliotou et al. 1998, 1999; Shitov 1999). Magnetic field strength expressed in the relativistic units,

$$b = \hbar e B / (m_e^2 c^3) \approx B / (4.414 \times 10^{13} \text{ G}), \quad (1)$$

is greater than unity for magnetars, unlike for ordinary pulsars.

The magnetic field affects thermodynamic and kinetic properties of dense degenerate plasmas in different ways, depending on density, temperature, and field strength (e.g., Yakovlev & Kaminker 1994). In general, electron motion transverse to the field is quantized into Landau orbitals. For sufficiently high temperature, however, the field can be treated as *non-quantizing* (classical). The non-quantizing magnetic field does not affect thermodynamic properties of matter, but hampers transverse transport and causes the Hall currents. In a *weakly quantizing* field, where electrons populate several Landau levels, the thermodynamic functions and kinetic coefficients oscillate with increasing density around their classical values. *Strongly quantizing* magnetic field confines most electrons to the ground Landau level. In this case, thermodynamic and kinetic properties of matter are very different from those in the classical regime.

The problem was extensively studied since the end of 1960s (Canuto & Ventura 1977 and references therein). Expressions for the kinetic coefficients, based on the solution of the Boltzmann equation in the relaxation-time approximation and valid for non-relativistic and relativistic electrons in the neutron star envelopes with quantizing magnetic fields were obtained by Kaminker & Yakovlev (1981) for transverse transport, by Yakovlev (1984) for longitudinal transport and by Hernquist (1984) for all cases. Potekhin (1996, hereafter Paper I) has shown that the usual description of electron transport along magnetic field with the Boltzmann equation yields almost the same transport coefficients as a more general kinetic equation for the electron spin density matrix. According to Paper I, the Debye–Waller factor enhances the longitudinal electrical and thermal conductivities near T_m much stronger if the magnetic field is quantizing. Basing on these results, Potekhin & Yakovlev (1996, hereafter Paper II) derived practical formulae for the longitudinal transport coefficients.

The studies cited above used the customary one-phonon approximation for the electron scattering in Coulomb solid. Recently Baiko et al. (1998) have reconsidered electron transport in non-magnetized plasmas by including multi-phonon processes, which have proved to give a contribution of similar magnitude (but opposite sign) as the Debye–Waller factor near T_m . Concerning the Coulomb liquid, Baiko et al. (1998) have suggested that incipient ordering of ions in the strong-coupling regime affects electron scattering; they have proposed an approximate treatment of this effect by modification of the static structure factor of ions. Both modifications (in the solid and liquid phases) change the kinetic coefficients near the melting point and drastically reduce their discontinuities at $T = T_m$. The new ion structure factors have been employed by Potekhin et al. (1999, hereafter Paper III) in calculations of electrical and thermal conductivities in the outer envelopes of neutron stars without magnetic fields. Numerical results in Paper III have been fitted by analytic expressions, derived in the relaxation-time approximation with the use of a specially adjusted effective scattering potential.

In this paper, the effective potential obtained in Paper III is applied to calculation of electron transport coefficients at arbitrary magnetic field strength, at temperatures $T \sim (10^5\text{--}10^9)$ K and densities $\rho \sim (10^3\text{--}10^{11})\text{g cm}^{-3}$ typical for the outer envelopes of neutron stars. Energy-dependent effective relaxation times, subject to thermal averaging, are obtained for electron transport parallel and perpendicular to the quantizing magnetic fields. In the case of non-quantizing fields, the usual semiclassical formulae (e.g., Urpin & Yakovlev 1980b) are utilized taking into account the results of Paper III.

The paper is composed as follows. In Sect. 2, we describe typical plasma parameters of interest. In Sect. 3, we express the electron transport coefficients through an effective scattering potential in the relaxation time approximation. In Sect. 4, we present analytic fits to the effective energy-dependent relaxation times related to longitudinal and transverse electron transport in quantizing magnetic fields. Sect. 5 illustrates the main features of the transport coefficients given by the present theory.

2. Magnetized degenerate matter

Consider a plasma composed of electrons (with charge $-e$) and a single ion species with charge Ze and mass $m_i \approx Am_u$ (where $m_u = 1.6605 \times 10^{-24}$ g is the atomic mass unit, and A is the atomic mass number). The complete pressure ionization occurs at high temperatures or high densities (e.g., at $\rho \gtrsim 22 Z^2 A \text{g cm}^{-3}$ in the non-magnetic case – see Potekhin et al. 1997). Whenever this assumption is violated, we will employ the mean-ion approximation, in which all ions in all ionization stages are replaced by a single species with some effective values of Z and A . Electrons are assumed to be degenerate and nearly free. The degeneracy implies $T < T_F \equiv (\epsilon_F - m_e c^2)/k_B$, where ϵ_F is the Fermi energy (including the rest energy, $m_e c^2$) and k_B is the Boltzmann constant. Degenerate electrons can be considered as nearly free, if their kinetic energy exceeds greatly a typical energy of electron-ion Coulomb attraction; in a non-magnetized plasma, this happens at $\rho \gg 10AZ \text{g cm}^{-3}$ (e.g., Pethick & Ravenhall 1995).

A degenerate electron gas can be characterized by the Fermi momentum p_F or wave number $k_F = p_F/\hbar$. Without any magnetic field, $k_F = k_{F0} \equiv (3\pi^2 n_e)^{1/3}$, where $n_e \approx \rho Z/(m_u A)$ is the electron number density. It is also convenient to introduce the “relativity parameter” (e.g., Shapiro & Teukolsky 1983)

$$x_r = \hbar k_{F0}/m_e c \approx 1.009 (\rho_6 Z/A)^{1/3}, \quad (2)$$

where $\rho_6 \equiv \rho/(10^6 \text{g cm}^{-3})$.

Let the magnetic field \mathbf{B} be directed along the z -axis. Then, using the Landau gauge of the vector potential, the quantum states of a free electron can be labelled by the y -coordinate of the electron guiding centre, the longitudinal electron momentum p_z , the Landau number n , and a spin variable s . The ground Landau level ($n = 0$) is non-degenerate with respect to the spin variable ($s = -1$, statistical weight $g_0 = 1$) while the other levels ($n > 0$) are doubly degenerate ($s = \pm 1$, $g_n = 2$).

It is convenient to write (Paper II)

$$n_e = \int_{m_e c^2}^{\infty} \mathcal{N}_B(\epsilon) \left(-\frac{\partial f_0}{\partial \epsilon} \right) d\epsilon, \quad (3)$$

where ϵ is the electron energy,

$$f_0(\epsilon) = \{ \exp [(\epsilon - \mu)/k_B T] + 1 \}^{-1} \quad (4)$$

is the Fermi–Dirac distribution, μ is the chemical potential (ϵ and μ include $m_e c^2$), and

$$\mathcal{N}_B(\epsilon) = \frac{m_e \omega_c}{2(\pi \hbar)^2} \sum_{n=0}^{n_{\max}} g_n p_n(\epsilon). \quad (5)$$

Here and hereafter, $\omega_c = eB/m_e c$ is the electron cyclotron frequency, $p_n(\epsilon)$ is the value of $|p_z|$ for an electron on the Landau level n , and n_{\max} is the maximum Landau number for a given energy ϵ . Since $\epsilon = (m_e^2 c^4 + c^2 p_z^2 + 2m_e c^2 \hbar \omega_c n)^{1/2}$, we have

$$p_n(\epsilon) = [(\epsilon/c)^2 - (m_e c)^2 - 2m_e \hbar \omega_c n]^{1/2} \quad (6)$$

and obtain n_{\max} as integer part of convenient (Paper I) dimensionless energy variable

$$\nu = p_0^2(\epsilon)/(2m_e \hbar \omega_c). \quad (7)$$

At $T \ll T_F$, the derivative $(-\partial f_0/\partial \epsilon)$ can be replaced by the delta function $\delta(\epsilon - \epsilon_F)$; in this case $n_e = \mathcal{N}_B(\epsilon_F)$. If $n_{\max} \gg 1$, the sum in Eq. (5) can be approximated by an integral, which gives the classical (field-free) result,

$$\mathcal{N}_0(\epsilon) = p_0^3(\epsilon)/(3\pi^2\hbar^3). \quad (8)$$

Electrostatic screening produced by electrons is characterized by the Thomas–Fermi wave number k_{TF} :

$$k_{TF}^2 = 4\pi e^2 \frac{\partial n_e}{\partial \mu} = 4\pi e^2 \int_{m_e c^2}^{\infty} \frac{\partial \mathcal{N}_B(\epsilon)}{\partial \epsilon} \left(-\frac{\partial f_0}{\partial \epsilon} \right) d\epsilon. \quad (9)$$

The field can be considered as non-quantizing if $T \gg T_B$, where (Yakovlev & Kaminker 1994)

$$T_B = \hbar\omega_g/k_B \approx 1.34 \times 10^8 (B_{12}/\gamma_r) \text{ K}, \quad (10)$$

$B_{12} = B/(10^{12} \text{ G})$, $\gamma_r = \sqrt{1 + x_r^2}$, and $\omega_g = eBc/\epsilon$ is the electron gyrofrequency (for $\epsilon = \epsilon_F$). In the non-quantizing fields, $T_F = T_r(\gamma_r - 1)$ and $(k_{TF}/2k_{F0})^2 \approx (\alpha_f/\pi)\gamma_r/x_r$, where $T_r \equiv m_e c^2/k_B \approx 5.93 \times 10^9 \text{ K}$ and $\alpha_f = e^2/\hbar c \approx 1/137$ is the fine-structure constant.

The opposite case of strongly quantizing field occurs at $T \ll T_B$ and $\rho < \rho_B$, where

$$\rho_B = Am_n n_B/Z \approx 7.045 \times 10^3 (A/Z) B_{12}^{3/2} \text{ g cm}^{-3}, \quad (11)$$

$n_B = (\pi\sqrt{2})^{-1} a_m^{-3}$, and $a_m = (\hbar c/eB)^{1/2}$ is the so called magnetic quantum length. In this case,

$$k_F = 2\pi^2 a_m^2 n_e = (4/3)^{1/3} (\rho/\rho_B)^{2/3} k_{F0}. \quad (12)$$

Therefore T_F is strongly reduced for $\rho \ll \rho_B$.

The state of the one-component plasma (OCP) of ions depends on the Coulomb parameter,

$$\Gamma = \frac{(Ze)^2}{k_B T a_i} \approx \frac{22.75 Z^2}{T_6} \left(\frac{\rho_6}{A} \right)^{1/3}, \quad (13)$$

where $a_i = [3/(4\pi n_i)]^{1/3}$ is the ion-sphere radius, $n_i = n_e/Z$ is the number density of ions, and $T_6 \equiv T/(10^6 \text{ K})$. In a weakly coupled OCP, $\Gamma \ll 1$, ions form the Boltzmann gas whose screening properties are characterized by the inverse Debye screening length,

$$q_D = \sqrt{3\Gamma}/a_i. \quad (14)$$

For $\Gamma \gtrsim 1$, the ions constitute a strongly coupled liquid. The liquid freezes into a Coulomb crystal at some $\Gamma = \Gamma_m$. For classical ions (whose zero-point quantum vibrations are negligible), $\Gamma_m \approx 175$, whereas strong zero-point vibrations suppress the freezing and increase Γ_m (Nagara et al. 1987). The freezing is completely suppressed in the so called quantum liquids, which exist at $x_r \gtrsim 0.18AZ^{7/3}$, as can be estimated from numerical simulations (Jones & Ceperley 1996). In general, the quantization of ionic motion is significant at $T \ll T_p$, where

$$T_p = \hbar\omega_p/k_B \approx 7.832 \times 10^6 (Z/A) \sqrt{\rho_6} \text{ K} \quad (15)$$

is the ion plasma temperature, $\omega_p = (4\pi Z^2 e^2 n_i/m_i)^{1/2}$ being the ion plasma frequency. We do not consider the quantum ion solids and liquids hereafter.

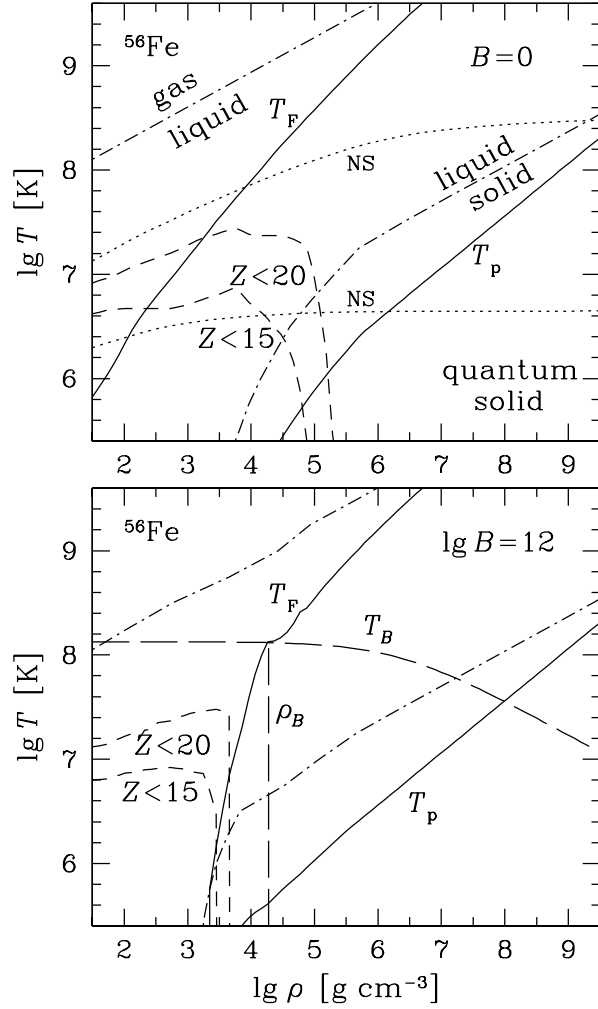


Fig. 1. Characteristic plasma domains on the ρ – T plane for iron. Upper panel: non-magnetic plasma; lower panel: $B = 10^{12} \text{ G}$. Solid lines show T_F and T_p vs. ρ ; upper and lower dot-dashed lines correspond to $\Gamma = 1$ and $\Gamma = 175$, respectively; short-dashed lines indicate the domains of partial ionization. Dotted lines on the upper panel show temperature profiles in the envelope of a “canonical” cooling neutron star (see text) for two values of the effective surface temperature, 2×10^5 and $2 \times 10^6 \text{ K}$. Long-dashed lines on the lower panel show T_B and ρ_B and separate the regions of strong and weak magnetic quantization.

We neglect also effects of magnetic field on the OCP of ions. This is justified if the ion cyclotron energy $\hbar\omega_{ci} = \hbar\omega_c Z m_e/m_i$ is small compared with either $k_B T$ [i.e., $T_6 \gg 0.0737 (Z/A) B_{12}$] or typical phonon energies in the OCP ($\sim \hbar\omega_p$; i.e., $\sqrt{\rho_6} \gg 0.0094 B_{12}$).

The characteristic ρ – T domains are shown in Fig. 1 for iron plasma at $B = 0$ and 10^{12} G . We have taken into account partial ionization in the mean-ion approximation. Electrons are degenerate below T_F ; ions are classical above T_p ; thus, strictly speaking, our consideration is valid in the stripe between the solid lines. In practice it may be reasonably accurate outside this stripe because it incorporates thermal averaging and because the quantum effects are actually small as long as $T \gtrsim 0.1 T_p$.

The short-dashed contours indicate the region of partial ionization: the upper contour corresponds to the effective charge $Z = 20$ and the lower one to $Z = 15$. We have evaluated Z in the same manner as Potekhin et al. (1997), requiring the equation of state (EOS) of a plasma composed of free electrons and ions with the effective charge Z to reproduce a “standard” EOS that takes into account partial ionization. In the non-magnetic case, the OPAL EOS (Rogers et al. 1996) has been adopted as such a standard and, whenever necessary, interpolated as explained in Potekhin et al. (1997). In the magnetic case, we have used the finite-temperature Thomas–Fermi EOS by Thorolfsson et al. (1998).

The dotted curves on the upper panel (marked “NS”) reproduce the temperature profiles (Potekhin et al. 1997)¹ in the envelope of a “canonical” neutron star of the mass $1.4 M_\odot$ and radius 10 km, with an effective surface temperature 2×10^5 K (the lower curve) and 2×10^6 K (the upper curve). In reality, effective temperatures of the middle-aged isolated neutron stars are believed to lie between these two extremes (e.g., Page 1998).

The dot-dashed lines on both panels correspond to $\Gamma = 1$ (gas/liquid smooth transition, upper lines) and $\Gamma = 175$ (liquid/solid phase transition, lower lines).

Finally, the long-dashed lines on the lower panel indicate three $\rho - T$ regions, where the magnetic field is strongly quantizing (to the left of ρ_B and considerably below T_B), classical (much above T_B), or weakly quantizing.

3. Transport coefficients

3.1. General relations

Consider electron electric and thermal currents induced in a magnetized plasma under the effect of an electric field \mathbf{E} and weak gradients of chemical potential $\nabla\mu$ and temperature ∇T . These currents can be decomposed into conduction and magnetization components (e.g., Hernquist 1984). The latter ones relate to surface effects and must be subtracted. Let \mathbf{j}_e and \mathbf{j}_T be the conduction components of electric and thermal current densities. They can be written as (e.g., Landau & Lifshitz 1960)

$$\mathbf{j}_e = \sigma \cdot \mathbf{E}^* - \alpha \cdot \nabla T, \quad \mathbf{j}_T = \tilde{\alpha} \cdot \mathbf{E}^* - \tilde{\kappa} \cdot \nabla T, \quad (16)$$

where $\mathbf{E}^* = \mathbf{E} + \nabla\mu/e$ is the electrochemical field. The symbols σ , α , $\tilde{\alpha}$, and $\tilde{\kappa}$ denote second-rank tensors (σ is the electrical conductivity tensor) which reduce to scalars at $B = 0$ only. From the Onsager symmetry relation one obtains: $\tilde{\alpha}_{ij}(\mathbf{B}) = T\alpha_{ji}(-\mathbf{B}) = T\alpha_{ij}(\mathbf{B})$.

Eqs. (16) can be rewritten as

$$\mathbf{E}^* = R \cdot \mathbf{j}_e - Q \cdot \nabla T, \quad \mathbf{j}_T = -TQ \cdot \mathbf{j}_e - \kappa \cdot \nabla T, \quad (17)$$

where $R = \sigma^{-1}$, $Q = -R \cdot \alpha$, and $\kappa = \tilde{\kappa} + T\alpha \cdot Q$ are the specific resistance, thermopower, and thermal conductivity tensors, respectively (here Q is defined as in Paper II; an opposite sign has been adopted by Hernquist 1984).

¹ We have recalculated the profiles using the updated non-magnetic conductivities (Paper III), but an effect of the update turned out to be negligible.

The components of σ , α , and $\tilde{\kappa}$ can be expressed as

$$\begin{bmatrix} \sigma_{ij} \\ \alpha_{ij} \\ \tilde{\kappa}_{ij} \end{bmatrix} = \int \begin{bmatrix} e^2 \\ e(\mu - \epsilon)/T \\ (\mu - \epsilon)^2/T \end{bmatrix} \frac{N_B(\epsilon)}{\epsilon/c^2} \tau_{ij}(\epsilon) \left(-\frac{\partial f_0}{\partial \epsilon} \right) d\epsilon. \quad (18)$$

The functions $\tau_{ij}(\epsilon)$ play role of relaxation times determined by electron scattering in the magnetic field. Owing to the symmetry properties of the tensors σ , α , and $\tilde{\kappa}$, there are only three different non-zero components: τ_{zz} related to longitudinal currents, $\tau_{xx} = \tau_{yy}$ related to transverse currents, and $\tau_{xy} = -\tau_{yx}$ related to the Hall currents.

3.2. Non-quantizing magnetic field

If the quantizing nature of the magnetic field is neglected, then (e.g., Urpin & Yakovlev 1980b)

$$\tau_{zz} = \tau_0, \quad \tau_{xx} = \frac{\tau_0}{1 + (\omega_g \tau_0)^2}, \quad \tau_{yx} = \frac{\omega_g \tau_0^2}{1 + (\omega_g \tau_0)^2}, \quad (19)$$

where τ_0 is the non-magnetic relaxation time, equal to an inverse effective collision frequency in this case.

In the outer envelopes of neutron stars, relaxation is mainly determined by electron-ion scattering. We restrict ourselves to consideration of this mechanism; possible inclusion of other processes is discussed briefly in Sect. 6. In strongly coupled Coulomb plasmas, the scattering is significantly affected by ion correlations. In the liquid phase, an appropriate structure factor of ions should be employed. In the solid phase, an adequate description is provided by the formalism of electron scattering off phonons with allowance for multi-phonon processes (see Baiko et al. 1998 for discussion and references). In both the liquid and solid regimes, it is convenient to write the squared Fourier transform of the scattering potential as

$$|U_q|^2 = (4\pi Z e^2)^2 |\phi_q|^2. \quad (20)$$

Here, ϕ_q is the so called screening function (which would be equal to q^{-2} for the Coulomb potential, were the screening neglected). Then

$$\tau_0(\epsilon) = \frac{p_0^2 v_0}{4\pi n_i Z^2 e^4 \Lambda_0(\epsilon)}, \quad (21)$$

where $v_0 = p_0 c^2 / \epsilon$ is an electron velocity, and $\Lambda_0(\epsilon)$ is the non-magnetic Coulomb logarithm. In strongly coupled, degenerate Coulomb plasmas, one has

$$\Lambda_0 = \int_0^{2p_0/\hbar} dq q^3 |\phi_q|^2 S(q) |F(q)|^2 \left[1 - \left(\frac{\hbar c q}{2\epsilon} \right)^2 \right], \quad (22)$$

where $F(q)$ is the form factor of ions, and $S(q)$ is an effective structure factor that describes the effects of ion correlations (Baiko et al. 1998).

In Paper III two forms of the effective Coulomb logarithm (Λ_σ and Λ_κ) have been obtained from calculations of σ and κ at $B = 0$ beyond the relaxation-time approximation. The latter approximation fails if inelastic processes with energy transfer

$\gtrsim k_B T$ are important. According to Baiko & Yakovlev (1995) and Paper III, this happens at low temperatures $T \ll T_p$. In this paper we will focus on the case $T \gtrsim T_p$, in which we can neglect the difference between Λ_κ and Λ_σ and adopt $\Lambda_0 = \Lambda_\sigma$ for $B = 0$.

The transport coefficients due to electron-ion and electron-phonon scatterings (in the Coulomb liquid and solid, respectively) can be described with a reasonable accuracy (Paper III) in a unified way under the conditions typical for the outer envelopes of neutron stars. For this purpose it is sufficient to replace $|\phi_q|^2 S(q) |F(q)|^2$ in Eq. (22) by the expression:

$$|\phi_q^{\text{eff}}|^2 = \frac{1 - e^{-w(q)}}{(q^2 + q_s^2)^2} G(t_p, \beta), \quad (23)$$

where

$$q_s^2 = (q_i^2 + k_{\text{TF}}^2) e^{-\beta}, \quad (24)$$

$$q_i^2 = q_D^2 (1 + 0.06 \Gamma) e^{-\sqrt{\Gamma}}, \quad (25)$$

$$w(q) = u_{-2} (q/q_D)^2 (1 + \beta/3), \quad (26)$$

$$G(t_p, \beta) = \frac{1 + 0.122\beta^2}{(1 + t_0^2/t_p^2)^{1/2}} D(t_p), \quad t_0 = \frac{0.19}{Z^{1/6}}. \quad (27)$$

In this case $e^{-w(q)}$ plays role of an effective Debye–Waller factor at large Γ and is negligible at $\Gamma \lesssim 1$; $u_{-2} = 13$, where u_j is $(\omega/\omega_p)^j$ averaged over phonon frequencies ω in a Coulomb crystal (e.g., Pollock & Hansen 1973); q_s is an effective screening wave number; and $G(t_p, \beta)$ is a phenomenological factor that describes reduction of the scattering rate, caused by quantum effects at $t_p \equiv T/T_p \ll 1$. The factors G , w , and q_s contain also phenomenological corrections to the Born approximation expressed through $\beta \equiv \pi\alpha_f Z p_{\text{FC}}/\epsilon_F$. Finally, the function $D(t_p) = \exp[-\alpha_0 u_{-1} \exp(-9.1 t_p)/4]$, where $\alpha_0 = 1.683 \sqrt{x_r/(AZ)}$ and $u_{-1} = 2.8$, is associated with quantum corrections to the Debye–Waller factor (Baiko & Yakovlev 1995). Note that one can safely set $G = 1$ for $T \gtrsim T_p$ and $Z \lesssim 30$.

3.3. Transport along quantizing magnetic field

Let us calculate the longitudinal electron transport coefficients in the quantizing magnetic field using the relaxation time approximation and the effective scattering potential determined by Eq. (23). According to Papers I and II, the longitudinal kinetic coefficients can be written in the form (18) by defining the effective relaxation time $\tau_{zz} = \tau_{\parallel}$ as

$$\frac{\mathcal{N}_B(\epsilon) c^2}{\epsilon} \tau_{\parallel}(\epsilon) = \frac{(eB)^2}{4\pi^3 \hbar Z^2 e^4 n_i} \Phi(\epsilon). \quad (28)$$

The dimensionless function $\Phi(\epsilon)$ is determined by a kinetic equation for the electron spin density matrix $\rho_{n s_1 s_2}(z, p_z)$. It has been shown in Paper I, however, that a good accuracy is provided by a simpler kinetic equation for the density distribution function $f_{ns} = \rho_{nss}$ in the “fixed spin” representation (Yakovlev 1984).

In order to obtain the longitudinal transport coefficients, it is sufficient to assume that \mathbf{E}^* and ∇T are collinear with \mathbf{B} . The electron distribution function can be sought in the form

$$f_{ns} = f_0 + l \text{sign}(p_z) \frac{\partial f_0}{\partial \epsilon} \left[eE^* + \frac{\epsilon - \mu}{k_B T} \frac{\partial T}{\partial z} \right] \varphi_{ns}(\epsilon), \quad (29)$$

where l is an appropriate scale length, and $\varphi(\epsilon)$ is a dimensionless function to be determined from the kinetic equation. The latter is reduced to an algebraic system (Yakovlev 1984):

$$\sum_{\gamma n' s'} a_{ns \rightarrow n' s'}^{(\gamma)}(\epsilon) [\varphi_{ns}(\epsilon) - \gamma \varphi_{n' s'}(\epsilon)] = 1. \quad (30)$$

Here, $a_{ns \rightarrow n' s'}^{(\gamma)}$ is a dimensionless scattering rate of an electron from a state with quantum numbers n and s into a state with quantum numbers n' and s' , with changed ($\gamma = -1$) or unchanged ($\gamma = 1$) direction of motion along \mathbf{B} . The summation is performed over $n' \leq n_{\text{max}}(\epsilon)$, $\gamma = \pm 1$, and $s' = \pm 1$ for $n' \geq 1$ (but $s' = -1$ if $n' = 0$). Note that the terms with $n' = n$, $s' = s$, and $\gamma = +1$ naturally vanish.

Since the scattering potential is written in the form (20), it is convenient to choose $l = m_e c^2 \hbar \omega_c / (2\pi n_i Z^2 e^4)$. Then (Yakovlev 1984)

$$\Phi(\epsilon) = \sum_{ns} \varphi_{ns}(\epsilon) \quad (31)$$

and²

$$a_{ns \rightarrow n' s'}^{(\gamma)}(\epsilon) = [4(\tilde{\epsilon} + 1)^2 \tilde{p}_n \tilde{p}_{n'}]^{-1} S_{nn' ss'}^{(\gamma)}(\tilde{\epsilon}), \quad (32)$$

where $\tilde{\epsilon} = \epsilon/m_e c^2$, $\tilde{p}_n = p_n/m_e c$,

$$\begin{aligned} S_{nn' 11}^{(\gamma)} &= [(\tilde{\epsilon} + 1)^2 + \gamma \tilde{p}_n \tilde{p}_{n'}]^2 Q_1 \\ &\quad + 4b^2 nn' Q_2 + 4b [(\tilde{\epsilon} + 1)^2 + \gamma \tilde{p}_n \tilde{p}_{n'}] \sqrt{nn'} Q_3, \\ S_{nn' 1, -1}^{(\gamma)} &= 2b [n' \tilde{p}_n^2 Q_1 + n \tilde{p}_{n'}^2 Q_2] - 4b\gamma \sqrt{nn'} \tilde{p}_n \tilde{p}_{n'} Q_3, \end{aligned}$$

and $S_{nn', -s, -s'}^{(\gamma)}$ differ from $S_{nn' ss'}^{(\gamma)}$ by interchanging Q_1 and Q_2 . Here the functions Q_i (Yakovlev 1984) are generalized to arbitrary scattering potential:

$$Q_1 = \int_0^\infty I_{n-1, n'-1}^2(u) \tilde{\phi}^2(u) du, \quad (33)$$

$$Q_2 = \int_0^\infty I_{nn'}^2(u) \tilde{\phi}^2(u) du, \quad (34)$$

$$Q_3 = \int_0^\infty I_{nn'}(u) I_{n-1, n'-1}(u) \tilde{\phi}^2(u) du, \quad (35)$$

where

$$I_{nn'}(u) = \left(\frac{n!}{n'} u^{n-n'} e^{-u} \right)^{1/2} L_n^{n-n'}(u) \quad (36)$$

is a Laguerre function (Sokolov & Ternov 1968; $L_n^m(u)$ are the associated Laguerre polynomials – e.g., Abramowitz & Stegun 1972), $\tilde{\phi}(u) = 2|\phi_q|/a_m^2$, and $(\hbar q)^2$ is set equal to $(p_n - \gamma p_{n'})^2 + 2(\hbar/a_m)^2 u$.

² Eq. (32) reproduces Eq. (26) of Yakovlev (1984) corrected for a misprint.

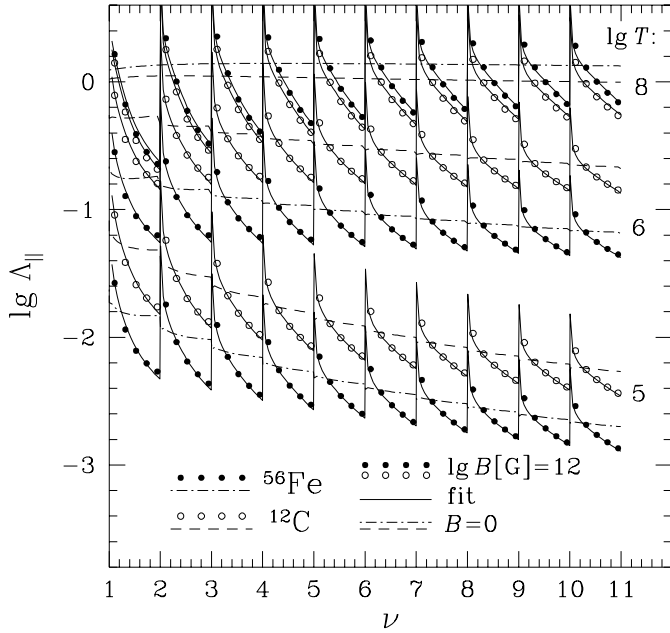


Fig. 2. Calculated (symbols) and fitted (solid lines) effective longitudinal Coulomb logarithms $\Lambda_{||}$ vs. dimensionless electron energy variable Eq. (7) for fully ionized iron (filled circles) and carbon (open circles) at $B = 10^{12}$ G and three values of temperature ($\lg T$ is given at the right end of each bunch of curves). Dot-dashed and dashed curves represent the field-free Coulomb logarithms Λ_0 for Fe and C from Paper III.

3.4. Transport perpendicular to quantizing magnetic field

Let us start with the case of large Hall parameter, $\tau_0 \omega_g \gg 1$. In this limit, as follows from Eq. (19),

$$\tau_{yx} \approx 1/\omega_g \quad \text{and} \quad \tau_{xx} \approx (\omega_g^2 \tau_0)^{-1}, \quad (37)$$

provided the magnetic field is non-quantizing. The case of quantizing field was considered by Kaminker & Yakovlev (1981) and Hernquist (1984). The expressions for the transport coefficients derived by these authors can be written in the form (18) by defining, in analogy with Eq. (37),

$$\tau_{yx} = 1/\omega_g \quad \text{and} \quad \tau_{xx} = (\omega_g^2 \tau_{\perp})^{-1}, \quad (38)$$

where

$$\frac{\mathcal{N}_B(\epsilon) c^2}{\epsilon} \frac{1}{\omega_g^2 \tau_{\perp}(\epsilon)} = \frac{Z^2 e^4 n_i}{2\pi \hbar^3 \omega_c^2} \Psi(\epsilon), \quad (39)$$

$$\Psi(\epsilon) = \sum_{nn'\gamma} \frac{b}{2\tilde{p}_n \tilde{p}_{n'}} \left[(\tilde{\epsilon}^2 + 1 + \gamma \tilde{p}_n \tilde{p}_{n'}) (Q_1^{\perp} + Q_2^{\perp}) + 4b \sqrt{nn'} Q_3^{\perp} \right], \quad (40)$$

and functions Q_i^{\perp} differ from Q_i [Eqs. (33)–(35)] by an additional factor u in each integrand.

In weakly quantizing magnetic field, $\tau_{\perp}(\epsilon)$ oscillates around $\tau_0(\epsilon)$; it can be replaced by $\tau_0(\epsilon)$ in the non-quantizing limit. This allows us to interpolate between the regimes of large and moderate-to-low Hall parameters using the formulae:

$$\tau_{xx} = \frac{\tau_{\perp}}{1 + (\omega_g \tau_{\perp})^2}, \quad \tau_{yx} = \frac{\omega_g \tau_{\perp}^2}{1 + (\omega_g \tau_{\perp})^2}. \quad (41)$$

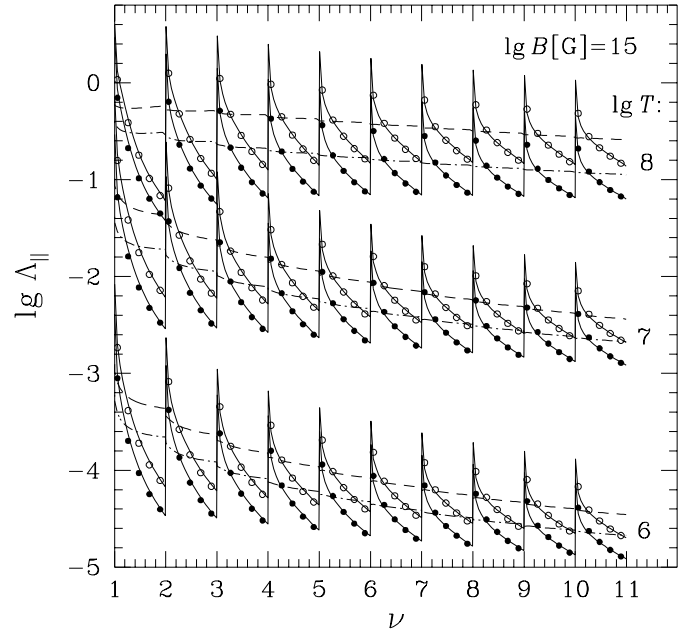


Fig. 3. Same as in Fig. 2 but for $B = 10^{15}$ G and different set of T .

Eqs. (41) relate the effective relaxation times τ_{xx} and τ_{yx} to the effective transverse electron collision frequency τ_{\perp}^{-1} and correctly reproduce the known limits (19) (non-quantizing field, arbitrary Hall parameter) and (38) (arbitrary field, large Hall parameter).

In addition, our interpolation (41) of τ_{xx} eliminates the well known divergency, that arises from direct substitution of Eq. (39) in the integrand of Eq. (18) because $\Psi(\epsilon)$ turns to infinity at each Landau threshold as $(\nu - n_{\max})^{-1}$. Previously $\Psi(\epsilon)$ was truncated at some level, estimated by a semi-qualitative analysis of physical processes that could, in principle, eliminate the divergency, were they included into the theory (Kaminker & Yakovlev 1981). One can show, however, that the derivation of expressions for the transverse transport coefficients [equivalent to our Eqs. (38)–(40)] implied that $\omega_g \tau_{\perp} \gg 1$. By correcting relations (38) in case where $\omega_g \tau_{\perp}$ is not very large, Eq. (41) ensures finiteness of τ_{xx} , thus making a truncation unnecessary.

4. Fitting formulae for $\tau_{||}(\epsilon)$ and $\tau_{\perp}(\epsilon)$

Explicit expressions of Q_i and Q_i^{\perp} for the function $|\phi_q^{\text{eff}}|^2$ in the form (23) are given in the Appendix. Using them, we have performed extensive calculations of $\tau_{||}$ and τ_{\perp} from Eqs. (28), (30)–(32) and (39). The key parameters of the function $|\phi_q^{\text{eff}}|$, which enters these expressions, – the Debye–Waller parameter $a_{\text{DW}} = w(2k_{\text{F}0}) \approx u_{-2} (2k_{\text{F}0}/q_{\text{D}})^2$ and the Coulomb screening parameter $a_s = (q_s/2k_{\text{F}0})^2$, – as well as the magnetic field parameter b , varied independently from 10^{-4} to 10^2 . For any value of b , the variable ν [related to ϵ via Eq. (7)] varied from 0 to 25, taking on 5–10 values over each interval $(n_{\max}, n_{\max} + 1)$.

Calculation is quite simple as long as $\nu < 1$, the functions $\Phi(\epsilon)$ and $\Psi(\epsilon)$ being given by Eqs. (A8)–(A10). For $\nu > 1$, we

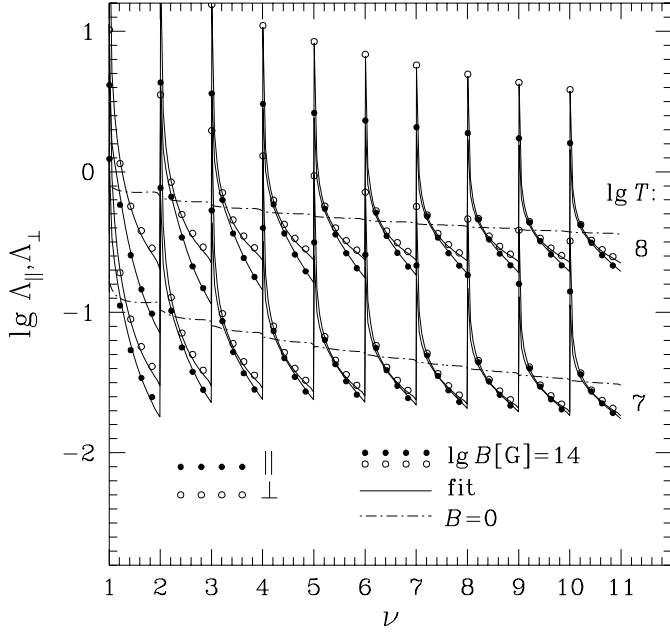


Fig. 4. Longitudinal ($\Lambda_{||}$, filled circles) and transverse (Λ_{\perp} , open circles) effective Coulomb logarithms in iron plasma for $B = 10^{14}$ G and two values of T . The solid lines show the fit; the dot-dashed lines show Λ_0 .

have fitted the results of our numerical calculations by analytic formulae.

Let us define longitudinal and transverse effective Coulomb logarithms $\Lambda_{||,\perp}(\epsilon)$ through the relations

$$\tau_{||}(\epsilon) = \frac{\mathcal{N}_0(\epsilon)}{\mathcal{N}_B(\epsilon)} \frac{p_0^2 v_0}{4\pi n_i Z^2 e^4 \Lambda_{||}(\epsilon)}, \quad (42)$$

$$\tau_{\perp}(\epsilon) = \frac{\mathcal{N}_0(\epsilon)}{\mathcal{N}_0(\epsilon)} \frac{p_0^2 v_0}{4\pi n_i Z^2 e^4 \Lambda_{\perp}(\epsilon)}. \quad (43)$$

As seen from Eq. (21), the functions $\Lambda_{||}$ and Λ_{\perp} turn into Λ_0 if the magnetic field is non-quantizing. In the quantizing fields, the ratios $\Lambda_{||}/\Lambda_0$ and $\Lambda_{\perp}/\Lambda_0$ are fitted by the expressions

$$\frac{\Lambda_{||}}{\Lambda_0} = \left\{ D \left[1 + \frac{\sqrt{b}}{\tilde{p}_0} \left(\frac{A}{x} - B\sqrt{x} + C \frac{x - \sqrt{x}}{n_{\max}} \right) \right]^{-2} + L^2 x^2 \left[\frac{3x^2 - 1}{2n_{\max} + 1.5x^2/(1+2b)^2} + 0.07 + \frac{E}{5} \right]^2 \right\}^{-1/2}, \quad (44)$$

$$\frac{\Lambda_{\perp}}{\Lambda_0} = 1 + \frac{b}{\tilde{p}_0^2} \frac{\tilde{A}}{x^2} + (\sqrt{b}/\tilde{p}_0) \left[(\tilde{B} \ln n_{\max}) x^{-1} - (\tilde{C} + \tilde{D} \ln n_{\max}) \sqrt{x} \right], \quad (45)$$

where $x = \tilde{p}_n/\sqrt{b} = \sqrt{2(\nu - n_{\max})}$,

$$A = \frac{30 - 15E - (15 - 6E)v_0^2}{30 - 10E - (20 - 5E)v_0^2},$$

$$B = \frac{3}{2} - \frac{E}{2} + \frac{1}{4} \frac{v_0^2}{1 - 2v_0^2/3}, \quad C = \frac{1 - E + 0.75v_0^2}{1 + v_0^2},$$

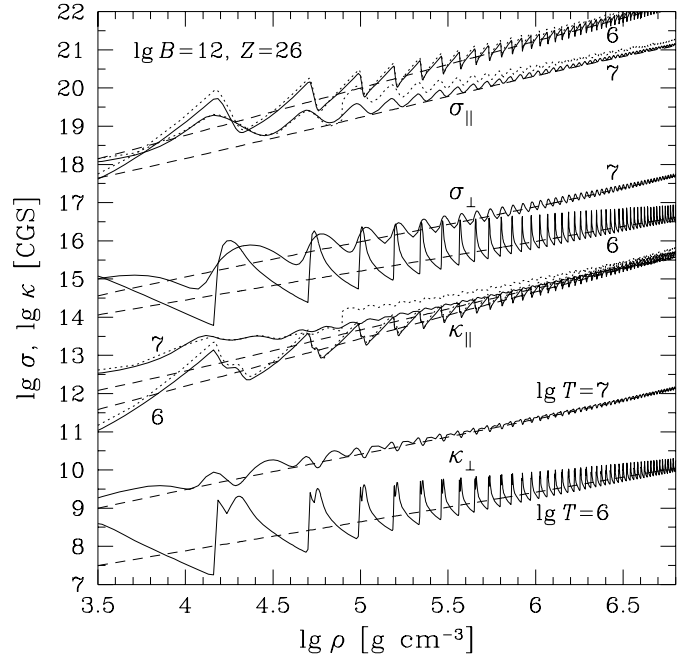


Fig. 5. Longitudinal ($||$) and transverse (\perp) electrical (σ) and thermal (κ) conductivities in the outer neutron-star envelope composed of iron for $B = 10^{12}$ G and two values of $\lg T$ (marked near the curves): comparison of the new results (solid lines) with the classical approximation [Eq. (19), dashed lines] and with the old results for the longitudinal conductivities (dotted lines) from Paper II.

$$D = 1 + 0.06 \frac{L^2}{n_{\max}^2}, \quad E = \frac{1 - \exp(-a_{\text{DW}})}{a_{\text{DW}}};$$

$$\tilde{A} = 0.8(1 + \tilde{L}) + 0.2L, \quad \tilde{B} = (0.68 - 1.3\tilde{E})\tilde{L}^{1/6},$$

$$\tilde{C} = 1.42 - \tilde{E} + \tilde{L}^{1/2}/3, \quad \tilde{D} = (0.52 - \tilde{E})\tilde{L}^{1/4},$$

$$\tilde{E} = (10 + 5/b)^{-1}, \quad L = \ln(1 + \tilde{a}^{-1}), \quad \tilde{L} = \tilde{a}L,$$

$$\tilde{a} = [\sqrt{a_s} + (2 + 0.5 a_{\text{DW}})^{-1}]^2.$$

The leading terms at $x \rightarrow 0$ are proportional to x^{-1} in Eq. (44) and x^{-2} in Eq. (45), reproducing the asymptotic behaviour of the functions Φ and Ψ . The accuracy of the fit was checked for $\nu - n_{\max} \geq 0.01$, which is quite sufficient for most applications. Eqs. (44) and (45) fit our numerical results with a typical error of a few percent. A maximum error up to 40% occurs only at some extreme values of a_s , a_{DW} , and ν . In addition, we have compared the new fit (44) with the one in Paper II (in the particular case of $a_{\text{DW}} \rightarrow \infty$ which corresponds to the screened Coulomb scattering potential considered in Paper II). On average, the new fit turned out to be more accurate than the old one.

Figs. 2–4 illustrate the accuracy of Eqs. (44) and (45) for realistic parameters in the neutron-star envelopes. In Figs. 2 and 3, the filled and empty circles represent $\Lambda_{||}(\epsilon)$ calculated from Eqs. (28) and (42); in Fig. 4 we have additionally plotted $\Lambda_{\perp}(\epsilon)$, obtained using Eqs. (39) and (43). The parameters a_s and a_{DW} have been calculated for fully ionized iron or carbon plasmas at various T from 10^5 to 10^8 K and B from 10^{12} to 10^{15} G

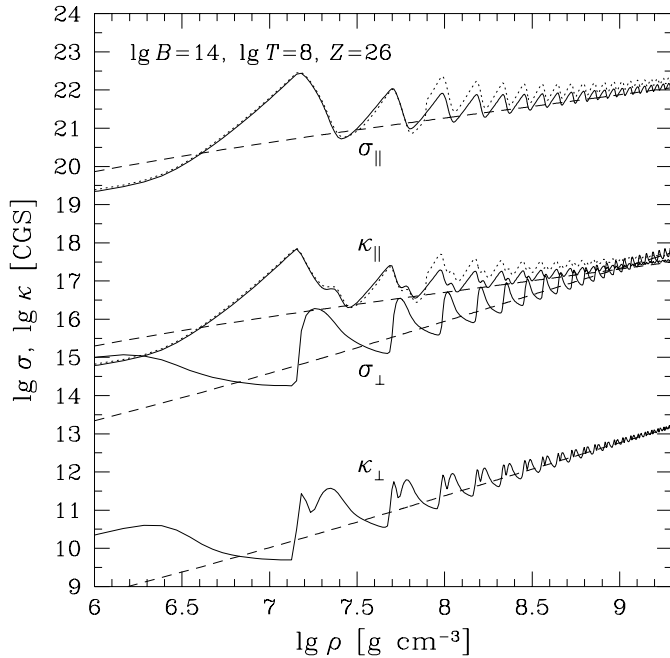


Fig. 6. Same as in Fig. 5 but for $B = 10^{14}$ G and $T = 10^8$ K.

(indicated in the figures). At every point, the plasma density has been determined from the condition $\epsilon_F = \epsilon(\nu)$ using Eq. (7). In all figures, the fits (44) or (45) are drawn by solid lines. The dashed and dot-dashed lines represent the non-magnetic Coulomb logarithm $\Lambda_0(\epsilon)$ given in Paper III.

Since our fitting formulae depend analytically on the parameters of the effective screening function (23), they need not be changed in case future refinement of the theory will cause modification of these parameters.

5. Numerical results for transport coefficients

Figs. 5 and 6 show electrical and thermal conductivities calculated with the effective relaxation times $\tau_{ij}(\epsilon)$ given by Eqs. (41)–(43) at various ρ , T , and B appropriate for outer envelopes of the neutron stars. The use of the analytic equations (A8)–(A10) for $\nu < 1$ and (44), (45) for $\nu > 1$ reduces numerical calculation to one-dimensional integration in Eq. (18), which has been performed using a fast algorithm described in Sect. 5 of Paper II.

The density range in every figures allows to see the strongly quantizing (below the first Landau threshold) and weakly quantizing regimes. The non-quantizing (classical) results are plotted by the dashed lines.

Fig. 5 shows the longitudinal and transverse conductivities in a neutron star envelope composed of iron for $B = 10^{12}$ G. The quantum oscillations around the classical values are more pronounced at lower temperatures. Fig. 6 illustrates the conductivities at stronger field, $B = 10^{14}$ G, which may be relevant to magnetars. The classical formulae correctly reproduce the large-scale trend of the curves and the reduction of transverse conductivities with respect to longitudinal ones. Nevertheless, deviations caused by the quantum oscillations are quite promi-

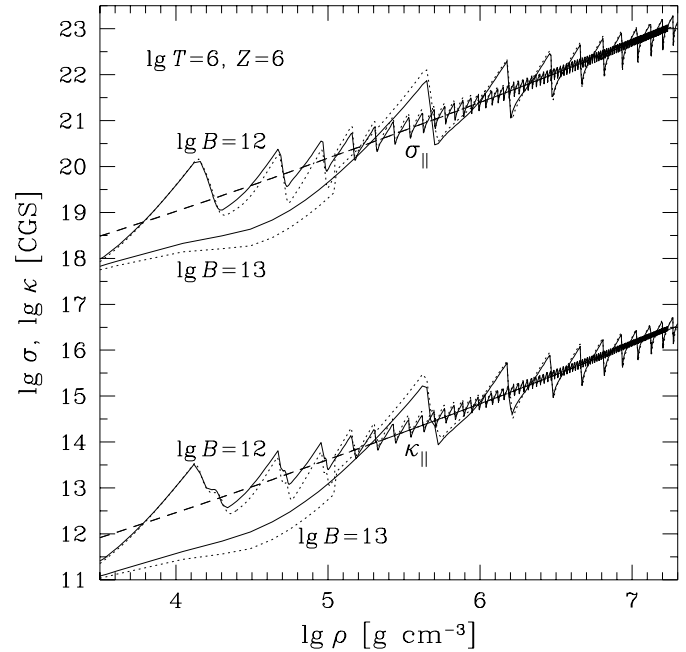


Fig. 7. Longitudinal conductivities for $Z = 6$ and $T = 10^6$ K at $B = 10^{12}$ and 10^{13} G. As in Figs. 5 and 6, the solid, dotted, and dashed lines show the new, old, and classical results, respectively.

nent, especially in the regime of strong quantization, where they may reach orders of magnitude.

For comparison, we have plotted (by dotted lines) the longitudinal conductivities calculated using the formalism of Paper II. The temperature values in Fig. 5 have been deliberately chosen the same as in Fig. 5 of Paper II (10^6 and 10^7 K). Note that for $T = 10^6$ K, the plasma is entirely within the solid crust. In this case, our old results agree nicely with the new ones. On the contrary, for $T = 10^7$ K in Fig. 5, as well as for $T = 10^8$ K in Fig. 6, the displayed density range extends into both the solid crust and liquid ocean of the star. The new conductivities go smoothly across the phase transition, whereas the old ones exhibit large jumps and appear to be significantly overestimated just behind the ocean/crust interface. This is caused by an overestimated effect of the Debye–Waller factor in Paper II, now corrected by including multi-phonon processes.

Fig. 7 shows the longitudinal conductivities of carbon plasma for $B = 10^{12}$ and 10^{13} G, which may chance, e.g., in a neutron star with an accreted carbon shell. In this case, the bottom of the ocean lies slightly above $\rho = 10^5 \text{ g cm}^{-3}$. Once again, we observe significant discontinuities of the “old” conductivities, which deviate from the new ones on both sides of the interface. The difference in the liquid phase is attributed to the modified ion structure factor used for obtaining $|\phi_q^{\text{eff}}|^2$ in Paper III, instead of a simplified screened-Coulomb model in the previous work.

In Fig. 8 we present the longitudinal and transverse components of the thermopower tensor for the sets of parameters used in Figs. 5, 6. The longitudinal thermopower from Paper II is shown by the dotted lines. Unlike the conductivities, the longitudinal thermopower did not possess considerable breaks at

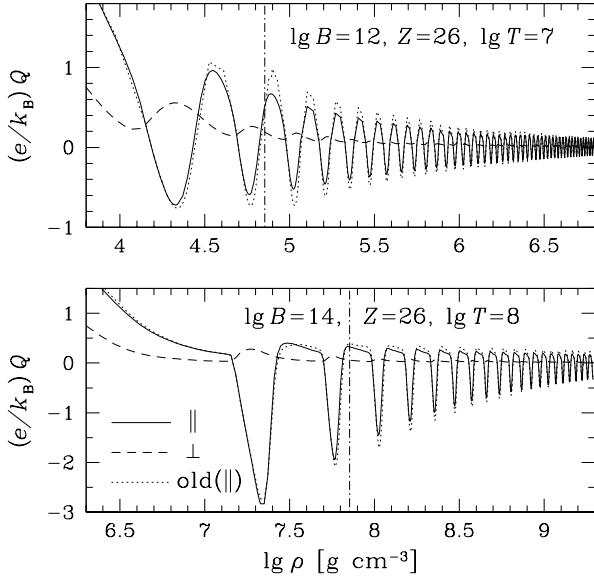


Fig. 8. Longitudinal (solid lines) and transverse (dashed lines) thermopower in units of k_B/e , for two sets of indicated parameters. For comparison, the dotted lines show the results of Paper II. Vertical dot-dashed lines indicate the liquid/solid phase transition.

the phase transitions in the old theory. Nevertheless, one can observe that the “new” results differ from the “old” ones. As in the previous figures, this difference is noticeable in the vicinity of the freezing point.

In the previous figures we have presented the longitudinal and transverse transport coefficients, which evince magnetic quantum oscillations around their classical values. The off-diagonal (Hall) electrical and thermal conductivities do not exhibit such oscillations and practically coincide with their non-magnetic counterparts given by Eqs. (18) and (19). Unlike them, the Hall component of the thermopower, Q_{yx} , does oscillate, as illustrated in Fig. 9 for iron plasma at $B = 10^{12}$ G and $T = 10^6$, 10^7 , and 10^8 K. The oscillations are very sharp at $T = 10^6$ K, but they are completely smeared out at the highest temperature, $T = 10^8$ K, which is close to T_B in the present example. The difference of vertical scales in Figs. 8 and 9 reflects that Q_{yx} is relatively small. Nevertheless, it may cause a variety of thermomagnetic effects in neutron star envelopes (Urpin et al. 1986).

6. Conclusions

We have derived practical expressions for the electron transport coefficients in degenerate ($T \lesssim T_F$) layers of neutron-star envelopes with magnetic fields which may be quantizing. Generally, these expressions require energy integration, Eq. (18). In the case of strongly degenerate electrons ($T \ll T_F$) and not too close to the Landau thresholds ($\nu - n_{\max} \gtrsim k_B T / \hbar \omega_g$), even this numerical integration becomes unnecessary, and the electrical conductivity reads $\sigma_{ij} \approx (e^2 n_e c^2 / \epsilon_F) \tau_{ij}(\epsilon_F)$, where τ_{ij} is provided by our analytic formulae, while the thermal

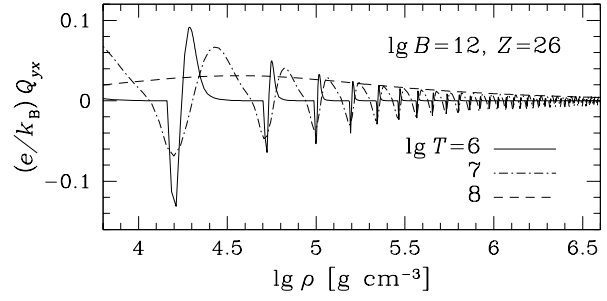


Fig. 9. Hall component of thermopower in units of k_B/e , for iron plasma at $B = 10^{12}$ G and three values of temperature.

conductivity is given by the Wiedemann–Franz law, $\kappa_{ij} \approx (\pi^2 k_B^2 T / 3e^2) \sigma_{ij}$.

We have used an effective potential, which has been obtained in Paper III assuming that the conductivities are determined by the electron scattering off ions (off phonons in the crystalline phase). It is well known (e.g., Yakovlev & Urpin 1980) that this is the main mechanism regulating electron transport at $T_p \lesssim T \lesssim T_F$. Other contributing mechanisms are the electron–electron scattering and scattering off lattice defects and impurities in the crystal. Corrections due to the impurity scattering can be introduced in a standard albeit approximate way by summation of relevant partial collisional frequencies, viz: $\tau_{\parallel, \perp}^{-1} = [\tau_{\parallel, \perp}^{\text{ei}}]^{-1} + [\tau_{\parallel, \perp}^{\text{imp}}]^{-1}$. In the case of charged impurities with charge number Z_{imp} , occasionally embedded in a Coulomb lattice, the effective scattering potential is again given by Eqs. (20) and (23), by setting $G = 1$, $e^{-w(q)} = 0$, and $q_i = 0$ and replacing Z by $|Z - Z_{\text{imp}}|$ and n_i by n_{imp} . Then $\tau_{\parallel, \perp}^{\text{imp}}$ are given by our formulae with an obvious modification of parameters.

We expect that our new formulae for the conductivities will be useful, in particular, in calculations of neutron-star thermal structure and evolution. It would be especially interesting to apply these results to investigating thermal structure of magnetars. Up to now, a very simplified analytic model (Heyl & Hernquist 1998) has been used in this case, but the problem deserves a more thorough study since it may provide a clue to the origin of the anomalous X-ray pulsars (Heyl & Hernquist 1997). The formulae presented here are almost as simple as those used by Heyl & Hernquist (1998), but they are accurate over a considerably broader range of plasma parameters.

The computer code that implements the formulae derived in the present paper is freely available from the author by electronic mail.

Acknowledgements. I am pleased to acknowledge the hospitality and financial support of the theoretical astrophysics group at the Ecole Normale Supérieure de Lyon, where a part of this work has been done. I am grateful to D.G. Yakovlev for his attention and useful discussions. I thank Frank Timmes for a useful advice concerning the computer code. This work was partially supported by INTAS Grant No. 96-542 and RFBR Grant No. 99-02-18099.

Appendix: calculation of auxiliary functions

Let us adopt Eq. (23) and set $G = 1$ for simplicity. Then the dimensionless function $\tilde{\phi}^2(u)$ that enters Eqs. (33)–(35) can be written as

$$\tilde{\phi}^2(u) = \frac{1 - e^{-\zeta(u+\xi)}}{(u + u_0)^2}, \quad (\text{A1})$$

where $\zeta = 2(a_m q_D)^{-2} u_{-2}(1 + \beta/3)$, $\xi = \frac{1}{2}(a_m/h)^2(p_n - \gamma p_n')^2$, $u_0 = \xi + \xi_s$, and $\xi_s = \frac{1}{2}(a_m q_s)^2$. Let us also define

$$Q_{jnn'm}^{(0)}(\xi, \zeta) = \int_0^\infty I_{nn'}(u) I_{n-j, n'-j}(u) \frac{e^{-\zeta(u+\xi)}}{(u+\xi)^m} du. \quad (\text{A2})$$

Then, for $j = 0$ or 1 , we have

$$Q_{2+j} = Q_{jnn'2}^{(0)}(u_0, 0) - e^{\zeta\xi_s} Q_{jnn'2}^{(0)}(u_0, \zeta), \quad (\text{A3})$$

$$Q_{2+j}^\perp = Q_{jnn'1}^{(0)}(u_0, 0) - u_0 Q_{jnn'2}^{(0)}(u_0, 0) - e^{\zeta\xi_s} \left[Q_{jnn'1}^{(0)}(u_0, \zeta) - u_0 Q_{jnn'2}^{(0)}(u_0, \zeta) \right], \quad (\text{A4})$$

and Q_1, Q_1^\perp are obtained from Q_2, Q_2^\perp by replacing $n \rightarrow n-1$ and $n' \rightarrow n'-1$.

For small Landau numbers ($n, n' \lesssim 10$), one can calculate $Q_{jnn'm}^{(0)}(\xi, \zeta)$ using an explicit expression of the Laguerre functions $I_{nn'}(u)$ in Eq. (A2). Since $I_{nn'}(u) = (-1)^{n'-n} I_{n'n}(u)$, we assume $n' \geq n$ without any loss of generality. Then

$$I_{n'n}(u) = e^{-u/2} u^{(n'-n)/2} \sum_{k=0}^n (-1)^k c_{n'nk} u^k, \quad (\text{A5})$$

where $c_{n'nk} = \sqrt{n!n!}/[k!(n-k)!(n'-n+k)!]$. For $j = 0$ or 1 ,

$$Q_{jn'nm}^{(0)}(\xi, \zeta) = \sum_{l=0}^{2n-j} (-1)^l \sum_{k=\max(0, l-n)}^{\min(n, l)} \left[\frac{n-k}{\sqrt{nn'}} \right]^j \times c_{n'nk} c_{n', n, l-k} (n' - n + l)! Q_{j, n' - n + l, 0, m}^{(0)}(\xi, \zeta), \quad (\text{A6})$$

$$Q_{j, n, 0, 1}^{(0)}(\xi, \zeta) = (1 + \zeta)^{-n} e^\xi E_{n+1}(\xi + \zeta\xi),$$

$$Q_{j, n, 0, 2}^{(0)}(\xi, \zeta) = (1 + \zeta)^{1-n} e^\xi [E_n(\xi + \zeta\xi) - E_{n+1}(\xi + \zeta\xi)];$$

an exponential integral $E_n(x) = \int_1^\infty t^{-n} e^{-xt} dt$ is easily calculated (Abramowitz & Stegun 1972).

In case where n or n' is large, Eq. (A6) is impractical because of approximate cancellations of positive and negative terms. In this case, one can use the following representation³

$$Q_{jn'nm}^{(0)}(\xi, \zeta) = \sum_{k=0}^{n-j} \frac{[n! (n')! (n-j)! (n'-j)!]^{1/2}}{k! (n-j-k)! (n'-j-k)!} \times \frac{1}{(m-1)! (j+k)!} \int_\zeta^\infty \frac{x^{2k+j} (x-\zeta)^{m-1}}{(1+x)^{n'+n-j+1}} e^{-\xi x} dx. \quad (\text{A7})$$

Finally, let us consider an important particular case of $n = n' = 0$. For transport along and across magnetic field,

³ Eq. (A7) generalizes Eq. (B8) of Paper I to the case in which ζ and $(m-1)$ may be non-zero simultaneously.

the effective inter-collision times $\tau_\parallel(\epsilon)$ and $\tau_\perp(\epsilon)$ are related to the functions $\Phi(\epsilon)$ and $\Psi(\epsilon)$ by Eqs. (28) and (39), respectively. From Eqs. (30)–(32) and (40), we obtain

$$\Phi(\epsilon) = \frac{\tilde{p}_0^2}{2 Q_\parallel(\xi)}, \quad \Psi(\epsilon) = \frac{b}{\tilde{p}_0^2} [\tilde{\epsilon}^2 Q^\perp(\xi) + Q^\perp(0)], \quad (\text{A8})$$

where

$$Q_\parallel(\xi) = u_0^{-1} (1 - e^{-\zeta\xi}) - e^{u_0} E_1(u_0) + (1 + \zeta) e^{u_0 + \zeta\xi_s} E_1(u_0 + \zeta u_0), \quad (\text{A9})$$

$$Q^\perp(\xi) = (1 + u_0) e^{u_0} E_1(u_0) - 1 + e^{-\zeta\xi} - (1 + u_0 + \zeta u_0) e^{u_0 + \zeta\xi_s} E_1(u_0 + \zeta u_0), \quad (\text{A10})$$

$\xi = 2\tilde{p}_0^2/b$, and the function E_1 is readily given by polynomial approximations (Abramowitz & Stegun 1972).

References

- Abramowitz M., Stegun I.A., 1972, In: Abramowitz M., Stegun I.A. (eds.) Handbook of Mathematical Functions. Dover, New York
- Baiko D.A., Yakovlev D.G., 1995, Astron. Lett. 21, 702
- Baiko D.A., Yakovlev D.G., 1996, Astron. Lett. 22, 708
- Baiko D.A., Kaminker A.D., Potekhin A.Y., Yakovlev D.G., 1998, Phys. Rev. Lett. 81, 5556
- Flowers E., Itoh N., 1976, ApJ 206, 218
- Canuto V., Ventura J., 1977, Fundam. Cosmic Phys. 2, 203
- Gottlieb E.V., Vasisht G., Dotani T., 1999, ApJ 522, L49
- Gudmundsson E.H., Pethick C.J., Epstein R.I., 1983, ApJ 272, 286
- Hernquist L., 1984, ApJS 56, 325
- Heyl J.S., Hernquist L., 1997, ApJ 489, L67
- Heyl J.S., Hernquist L., 1998, MNRAS 300, 599
- Hubbard W., Lampe M., 1969, ApJS 18, 297
- Itoh N., Mitake S., Iyetomi H., Ichimaru S., 1983, ApJ 273, 774
- Itoh N., Kohyama Y., Matsumoto N., Seki M., 1984, ApJ 285, 758
- Itoh N., Hayashi H., Kohyama Y., 1993, ApJ 418, 405
- Jones M.D., Ceperley D.M., 1996, Phys. Rev. Lett. 76, 4572
- Kaminker A.D., Yakovlev D.G., 1981, Theor. Math. Phys. 49, 1012
- Konar S., Bhattacharya D., 1997, MNRAS 284, 311
- Kouveliotou C., Dieters S., Strohmayer T., et al., 1998, Nat 393, 235
- Kouveliotou C., Strohmayer T., Hurley K., et al., 1999, ApJ 510, L115
- Landau L.D., Lifshitz E.M., 1960, Electrodynamics of Continuous Media. Pergamon, Oxford
- Miralles J., Urpin V., Kononov D., 1998, ApJ 503, 368
- Muslimov A., Page D., 1996, ApJ 458, 347
- Nagara H., Nagata Y., Nakamura T., 1987, Phys. Rev. A 36, 1859
- Nandkumar R., Pethick C.J., 1984, MNRAS 209, 511
- Page D., 1997, ApJ 479, L43
- Page D., 1998, Thermal evolution of isolated neutron stars. In: Buccheri R., van Paradijs J., Alpar M.A. (eds.) The Many Faces of Neutron Stars. Kluwer, Dordrecht, p. 539
- Pethick C.J., Ravenhall D.G., 1995, Annu. Rev. Nucl. Sci. 45, 429
- Pollock L.E., Hansen J.P., 1973, Phys. Rev. A 8, 3110
- Potekhin A.Y., 1996, A&A 306, 999; erratum 1997, A&A 327, 441 (Paper I)
- Potekhin A.Y., Yakovlev D.G., 1996, A&A 314, 341; erratum 1997, A&A 327, 442 (Paper II)
- Potekhin A.Y., Chabrier G., Yakovlev D.G., 1997, A&A 323, 415
- Potekhin A.Y., Baiko D.A., Haensel P., Yakovlev D.G., 1999, A&A 346, 345 (Paper III)
- Raikh M.E., Yakovlev D.G., 1982, Ap&SS 87, 193

- Rogers F.J., Swenson F.J., Iglesias C.A., 1996, *ApJ* 456, 902
- Shapiro S.L., Teukolsky S.A., 1983, *Black Holes, White Dwarfs, and Neutron Stars. The Physics of Compact Objects*. Wiley, New York
- Shibazaki N., Murakami T., Shaham J., Nomoto K., 1989, *Nat* 342, 656
- Shitov Yu.P., 1999, *IAUC* 7110
- Sokolov A.A., Ternov I.M., 1968, *Synchrotron Radiation*. Akademie, Berlin
- Taylor J.H., Manchester R.N., Lyne A.G., 1993, *ApJS* 88, 529
- Thompson C., Duncan R.C., 1995, *MNRAS* 275, 255
- Thorolfsson A., Rögnvaldsson Ö.E., Yngvason J., Gudmundsson E.H., 1998, *ApJ* 502, 847
- Urpin V., Konenkov D., 1997, *MNRAS* 292, 167
- Urpin V.A., Yakovlev D.G., 1980a, *SvA* 24, 126
- Urpin V.A., Yakovlev D.G., 1980b, *SvA* 24, 425
- Urpin V.A., Levshakov S.A., Yakovlev D.G., 1986, *MNRAS* 219, 703
- Vasisht G., Gotthelf E.V., 1997, *ApJ* 486, L129
- Yabe T., Shibazaki N., Hanami H., 1991, *PASJ* 43, L51
- Yakovlev D.G., 1984, *Ap&SS* 98, 37
- Yakovlev D.G., Kaminker A.D., 1994, Neutron star crusts with magnetic fields. In: Chabrier G., Schatzman E. (eds.) *The Equation of State in Astrophysics*. Cambridge Univ. Press, Cambridge, p. 214
- Yakovlev D.G., Urpin V.A., 1980, *SvA* 24, 303